ELSEVIER

Journal of Alloys and Compounds 231 (1995) 639–644

Journal of ALLOYS AND COMPOUNDS

Electrochemical and surface properties of iron-containing AB_5-type alloys

F. Meli, A. Züttel, L. Schlapbach

Institute of Physics, University of Fribourg, CH-1700 Fribourg, Switzerland

Abstract

$LaNi_5$-type metal hydride electrodes can attain a long cycle life in rechargeable batteries by partial substitution of Ni by expensive Co. We have investigated the surface and electrochemical properties of $(La,Mm)Ni_{5-x}(Fe,Al,Mn,Cu)_x$-type alloys with regard to battery applications. We found that partial substitution of nickel by iron did not increase the durability of $LaNi_5$. The initial capacity of $LaNi_{4.5}Fe_{0.5}$ was 320 mAh g^{-1}, while after 200 charge–discharge cycles it decreased to 130 mAh g^{-1}. With the combined substitution of iron and aluminium the durability increased. A more dramatic improvement to the stable alloys was attained for mischmetal- based alloys (e.g. $MmNi_{3.6}Fe_{0.7}Al_{0.3}Mn_{0.4}$). Deep discharges and cycling at 40°C caused only a minor capacity decrease for these alloys.

Surface analysis using X-ray photoelectron spectroscopy (XPS) of $LaNi_4Fe$ and $LaNi_{4.2}Fe_{0.5}Al_{0.3}$ showed significant changes in the surface composition of electrochemically cycled alloys. The surface changed from being lanthanum oxide rich to nickel rich. No aluminium or iron enrichment was found in the cycled alloys. The content of metallic nickel was lower than observed previously on the surface of $LaNi_{1-x}Si_x$ alloys. $LaNi_{4.2}Fe_{0.5}Al_{0.3}$ with good cyclic stability also showed a higher metallic Ni content in the subsurface layer. For all analysed samples, lanthanum was oxidized almost throughout the entire sputtering depth, whereas nickel became metallic at a depth of 0 to 60 Å and iron at a depth of 50 to 400 Å.

Keywords: Surface properties; Electrochemical properties; Iron substitutions; Battery; Electrodes

1. Introduction

Ni–MH battery production has increased rapidly. Ni–MH battery sales at the end of 1994 were estimated to reach 10% of the world Ni–Cd market. The use of an electrochemically stable metal hydride electrode has allowed the devlopment of rechargeable batteries which have a high capacity and are free of cadmium [1,2a]. Hydride-forming intermetallic compounds of the $LaNi_5$ family have a high surface activity and therefore allow a high charge–discharge rate. To obtain a long electrochemical cycle life, multicomponent alloys have been developed, e.g. $Mm(Ni,Co,Al,Mn)_5$-type alloys [2b].

Partial substitution of nickel by iron has been shown to lower the plateau pressure of $LaNi_5$- and $MmNi_5$-type alloys [3–5]. Iron is always present in mischmetal (Mm) and has been considered as an "impurity" because of its negative effect on the positive nickel hydroxide electrode. It reduces the overvoltage for oxygen evolution, resulting in a poor chargeability of the battery. However, this effect is not explicit. Ohta et al. [6] have found a higher utilization of nickel hydroxide electrodes containing 1% Fe_2O_3 additive at higher temperatures. Moreover, if the negative electrode is corrosion stable (no loss of iron), a high iron content in the negative electrode may be tolerated.

In most commercial AB_5-based battery electrode alloys, cobalt is the most expensive element. It has been stated that cobalt is indispensable to obtain a high cyclic stability, although its role is not yet fully understood. Iron, which is relatively inexpensive, is a 3d transition metal like nickel and cobalt. It is not known whether it may play a similar role to cobalt. If iron could be used to replace expensive cobalt entirely or partly, up to about one-third of the alloy raw material costs would be saved. Furthermore, iron-containing mischmetals are inexpensive and abundant.

SSDI 0925-8388(95)01744-5

Also alloy recycling would be easier if a certain iron content could be tolerated.

Therefore we have studied the electrochemical stability and surface properties of iron-containing, cobalt-free, multicomponent AB_5-type alloys. In this paper, we report the electrochemical measurements and X-ray photoelectron spectroscopy (XPS) surface analysis.

2. Experimental details

All intermetallic compounds were prepared by r.f. levitation melting of the appropriate amounts of the elements under an argon atmosphere of 10 kPa in a water-cooled copper crucible. The mischmetal (Mm, 98%) composition was 54% La, 27.5% Ce, 12.2% Nd and 5.3% Pr. All samples were rapidly cooled by switching off the r.f. field so that they dropped into the crucible (solidification in 2–3 s). They were then annealed at 1050°C for 1 h in vacuum ($p < 10^{-4}$ Pa). The crushed ingots were ground to an average grain size of about 100 μm. These samples will be referred to as "original".

For the electrochemical cycle life measurements, approximately 27 mg of active material was mixed with copper powder (Merck p.a.) in a weight ratio of 1:3 and pressed into a pellet ($d = 7$ mm, $p = 5 \times 10^8$ Pa). To obtain a copper-free pellet for surface analysis with XPS, about 70 mg of the sample alloy was pressed into a high void nickel foam and clamped between two fine nickel meshes. The electrodes were electrochemically charge–discharge cycled in a 6 M KOH electrolyte using an open half cell. The nickel counterelectrode was placed in a separate compartment of the cell. Unless otherwise mentioned, the end of the discharge was set to −0.6 V with respect to an Hg/HgO/6 M KOH reference electrode. Pulsed charging and discharging currents were used to measure the equilibrium electrode potential curves which were converted into "electrochemical pressure–composition–temperature (P–C–T) curves" as described previously [7]. For the surface analysis, electrochemically cycled samples were rinsed with twice distilled water, dried in rough vacuum, pressed into a pellet and introduced into the ultrahigh vacuum of the photoelectron spectrometer.

P–C isotherms were measured using the continuous method [8] with alloy samples of 2 g at a constant hydrogen flow of 2 ncm^3 H_2 min^{-1} (ncm^3, normal cm^3, $T = 0$°C, $p = 101.33$ kPa).

The relative concentration of the elements and their chemical state at the surface were analysed by XPS and sputter depth profiling as described previously [8].

3. Results and discussion

3.1. Electrochemical measurements

3.1.1. Cycle life measurements

We first measured the influence of the partial substitution of nickel with iron in $LaNi_5$ ($LaNi_{5-x}Fe_x$, $x = 0.5$ or 1). Electrochemical charge–discharge cycling in open half cells at 25°C showed no increase in the cyclic stability compared with $LaNi_5$. The addition of aluminium in $LaNi_{4.2}Fe_{0.5}Al_{0.3}$ resulted in a slightly better cyclic stability. All three alloys demonstrated a good discharge rate capability. This can be seen in the small additional discharge capacity using a discharge current ten times lower than during a normal discharge. The maximum capacities of 330–340 mAh g^{-1} were reached after about ten activation cycles (Fig. 1).

$MmNi_5$-based alloys containing iron exhibited higher cyclic stabilities than the $LaNi_5$-based alloys (Fig. 2). Both $MmNi_{3.6}Fe_{0.7}Al_{0.3}Mn_{0.4}$ and $MmNi_{3.7}Fe_{0.7}Al_{0.5}Cu_{0.1}$ had a maximum capacity of 280 mAh g^{-1}. The first composition was derived from an AB_5-type compound proposed by Ogawa et al. [2b] by replacing cobalt with iron, while the second compound was proposed by Hasegawa et al. [9]. The alloys differed strongly from each other in their rate capability. The capacities at the high discharge current decreased more strongly with the number of charge–discharge cycles than the capacities obtained with the additional low current discharges. This result could be due to a passivation effect [10].

To investigate how sensitive these alloys were to passivation, the cyclic stability of $MmNi_{3.6}Fe_{0.7}Al_{0.3}Mn_{0.4}$ was measured under deep discharges. At each cycle, an additional discharge with a low current was made (Fig. 3). Two different discharge cut-off po-

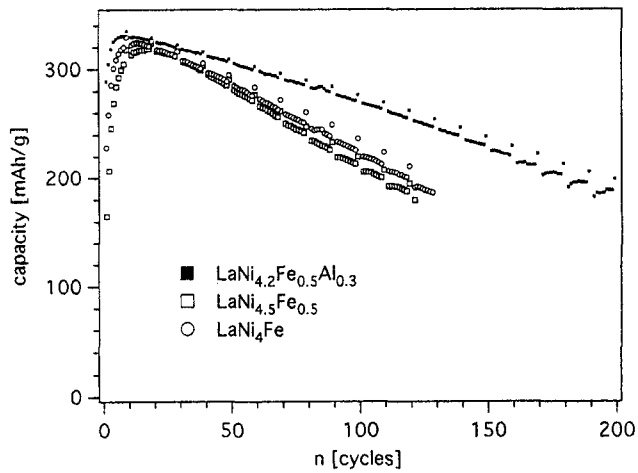

Fig. 1. Influence of iron on the discharge capacity vs. cycle number at 25°C. Charge and discharge currents were 150 mA g^{-1}. At every tenth cycle an additional discharge of 15 mA g^{-1} was performed.

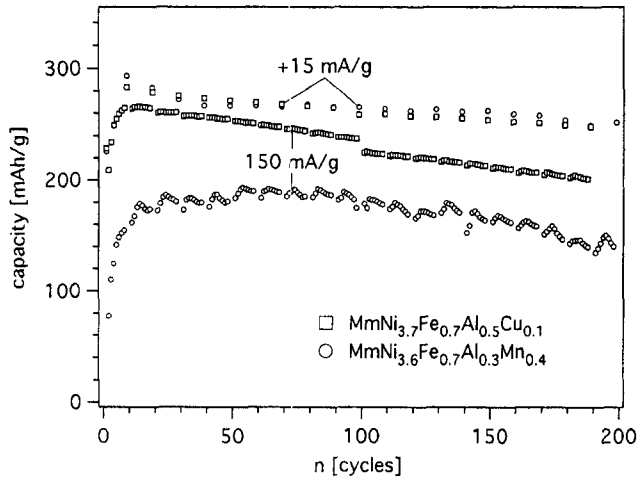

Fig. 2. Discharge capacity vs. cycle number of mischmetal-based, iron-containing, cobalt- free, AB_5-type alloys at 25°C. Charge and discharge currents were 150 mA g^{-1}. At every tenth cycle an additional discharge of 15 mA g^{-1} was performed. (At cycle 100, the discharge current was doubled for the $MmNi_{3.7}Fe_{0.7}Al_{0.5}Cu_{0.1}$ alloy.)

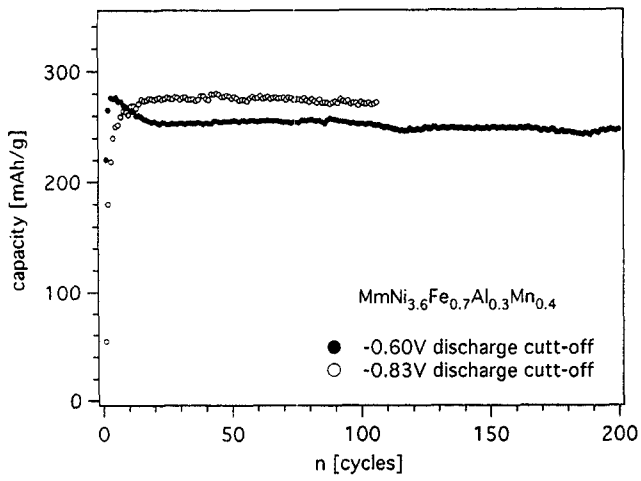

Fig. 3. Influence of the final discharge cut-off potential on the cycle life of the $MmNi_{3.6}Fe_{0.7}Al_{0.3}Mn_{0.4}$ alloy at 25°C. The charge current was 150 mA g^{-1} and the discharge current was 150 mA g^{-1} with an additional deep discharge of 15 mA g^{-1} at each cycle.

tentials were used (−0.6 V and −0.83 V vs. Hg/HgO). Under these discharge conditions, both electrodes showed no decrease in capacity with cycling. Interestingly, the measurement with the discharge to −0.83 V had a higher capacity, taking twice as much time compared with the discharge to −0.6 V. Due to the low rate capability of this alloy, a considerable amount (about one-third) of the capacity obtained at the high discharge current lies in the potential range of −0.83 to −0.6 V. Surprisingly, for an additional discharge with a current of only 15 mA g^{-1} to −0.6 V at each cycle, the alloy showed no capacity decrease and therefore neither corrosion nor loss of iron occurred.

In large prismatic cells, a considerable temperature increase may occur [11] which accelerates the processes of corrosion and passivation [1,10,12]. Therefore tests of the cyclic stability were also made at 40°C. Fig. 4 shows the results for $LaNi_{4.2}Fe_{0.5}Al_{0.3}$ and $MmNi_{3.6}Fe_{0.7}Al_{0.3}Mn_{0.4}$ alloys. The $LaNi_{4.2}Fe_{0.5}Al_{0.3}$ alloy showed a stronger capacity decrease at 40°C than at room temperature, while the capacity decrease of the $MmNi_{3.6}Fe_{0.7}Al_{0.3}Mn_{0.4}$ alloy remained almost unchanged. Only after approximately 100 cycles did the $MmNi_{3.6}Fe_{0.7}Al_{0.3}Mn_{0.4}$ alloy show a tendency to passivation. This can be seen in the increasing difference between the high and low current discharge capacity.

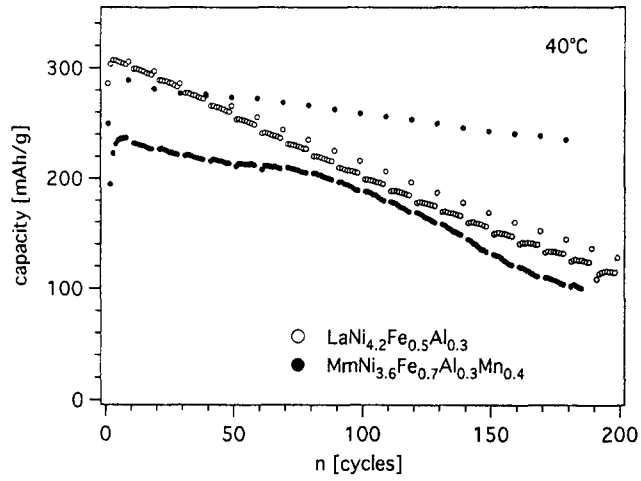

Fig. 4. Discharge capacity vs. cycle number for $LaNi_{4.2}Fe_{0.5}Al_{0.3}$ and $MmNi_{3.6}Fe_{0.7}Al_{0.3}Mn_{0.4}$ at 40°C. Charge and discharge currents were 150 mA g^{-1}. At every tenth cycle an additional discharge of 15 mA g^{-1} was performed.

3.1.2. Electrochemical P–C isotherm (PCI) measurements

Electrochemical PCI discharge curves were measured after 20 activation cycles at 25°C (Fig. 5). They

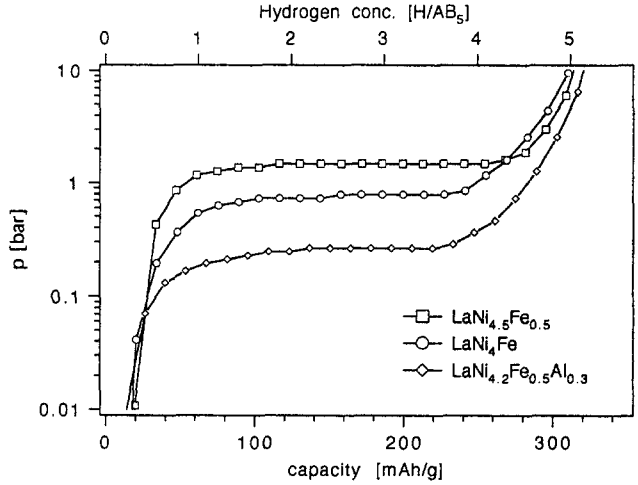

Fig. 5. Electrochemically measured PCI curves at 25°C for $LaNi_{4.5}Fe_{0.5}$, $LaNi_4Fe$ and $LaNi_{4.2}Fe_{0.5}Al_{0.3}$ with a pulsed discharge.

show that the plateau pressures decrease with iron and aluminium substitutions of nickel. While the plateaux become shorter with a higher iron content, the solubility of hydrogen in the β phase becomes larger. Therefore all alloys have nearly the same capacity at $p = 1$ MPa. For $LaNi_{4.2}Fe_{0.5}Al_{0.3}$, the plateau pressure was well below 1 bar making this alloy suitable for closed cell applications.

3.2. Pressure–composition isotherms

We compared the desorption curve of $LaNi_4Fe$ with those of $LaNi_4Co$ and $LaNi_5$ to gain an understanding of the phase changes involved. Fig. 6 shows the dynamically measured PCI curves for desorption at 40°C. The $LaNi_5$ curve shows a very flat desorption plateau. The transition from the α to the β phase occurs with a concentration change of 5.3 H/AB_5. The plateau pressure decreases with cobalt and iron substitutions in the order Ni > Co > Fe. The plateaux become shorter ($H/AB_5 = 3.3$) and the slopes are somewhat steeper compared with $LaNi_5$. The α phase (solid solution) of $LaNi_4Fe$ is slightly more extended. For the iron- substituted alloy, the β single phase begins at $H/AB_5 = 4$. The cobalt-substituted alloy has a transition to a short second plateau at $H/AB_5 = 3.5$, leading into the β single phase. Both the iron- and cobalt-substituted alloys have an increased hydrogen solubility in the β single phase. Iron substitution causes a small decrease in hydrogen gas storage capacity. At 25°C and 4 bar this capacity corresponds well to the electrochemically measured capacity of 310 mAh g^{-1}.

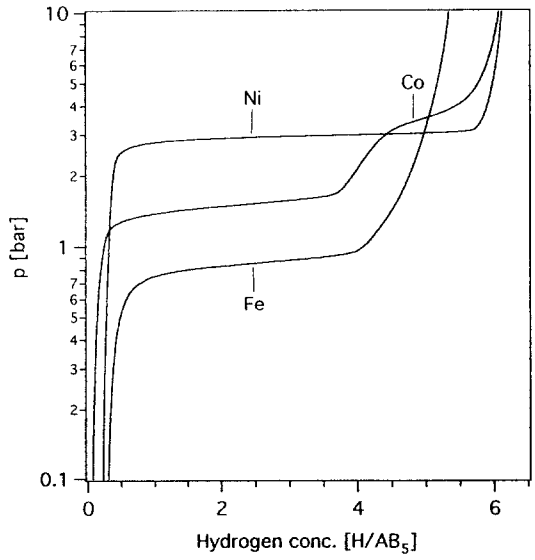

Fig. 6. Dynamic desorption pressure–composition isotherms for the $LaNi_4M$ system (with M ≡ Ni, Co, Fe) at 40°C measured with a constant H_2 flow rate of 1 ncm^3 min^{-1} (g alloy)$^{-1}$.

3.3. Surface analysis

The surfaces of powder pellets of the alloys $LaNi_4Fe$ and $LaNi_{4.2}Fe_{0.5}Al_{0.3}$ were analysed using XPS in the original state and after 30 electrochemical cycles. Fig. 7 shows the oxygen concentration at the surface of the different samples. After electrochemical cycling, the oxygen concentration increased as the capacity decreased. Lanthanum was oxidized almost throughout the entire sputtered depth, whereas nickel became metallic at a depth of 0 to 60 Å and iron at a depth of 50 to 400 Å for all samples analysed (Fig. 10, see below). The sputter rate used for depth profiling was about 4 Å min^{-1}.

The original alloys showed a strong lanthanum oxide enrichment at the surface as was observed in previous studies [13]. No iron enrichment was observed for either alloy (Figs. 8 and 9, top graphs). The $LaNi_{4.2}Fe_{0.5}Al_{0.3}$ alloy showed a small aluminium enrichment at the surface. The $LaNi_4Fe$ alloy showed very little nickel at the top surface and this nickel was already metallic. The aluminium-containing alloy showed a slightly higher nickel concentration at the top surface and a thin nickel oxide layer of about 10 Å was observed (Fig. 10, top graph).

After 30 electrochemical cycles (Figs. 8 and 9, bottom graphs), the nickel enrichment was not as pronounced as observed previously for $LaNi_{5-x}Si_x$ alloys [14]. The nickel concentration at the surface started slightly below bulk values and reached nominal concentrations at about 500 Å (where lanthanum becomes partly metallic). The more stable $LaNi_{4.2}Fe_{0.5}Al_{0.3}$ alloy showed higher nickel concentration in the near-surface layer. No aluminium or iron

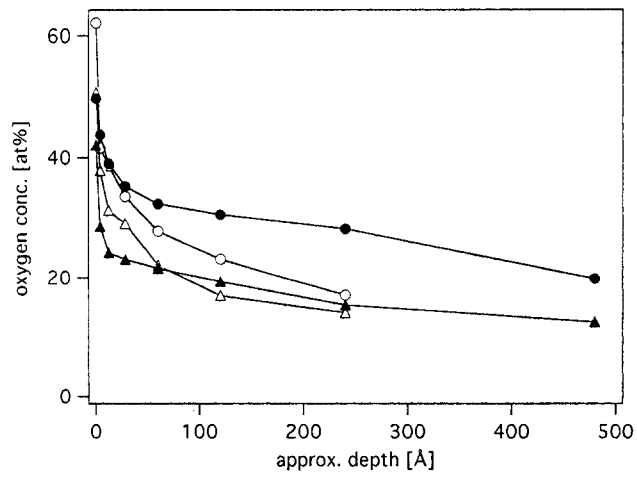

Fig. 7. XPS sputter depth profiles showing the oxygen penetration depth for $LaNi_4Fe$ (circles) and $LaNi_{4.2}Fe_{0.5}Al_{0.3}$ (triangles). The open symbols denote the original alloy and the filled symbols denote the alloy powders which have been electrochemically charge–discharge cycled 30 times.

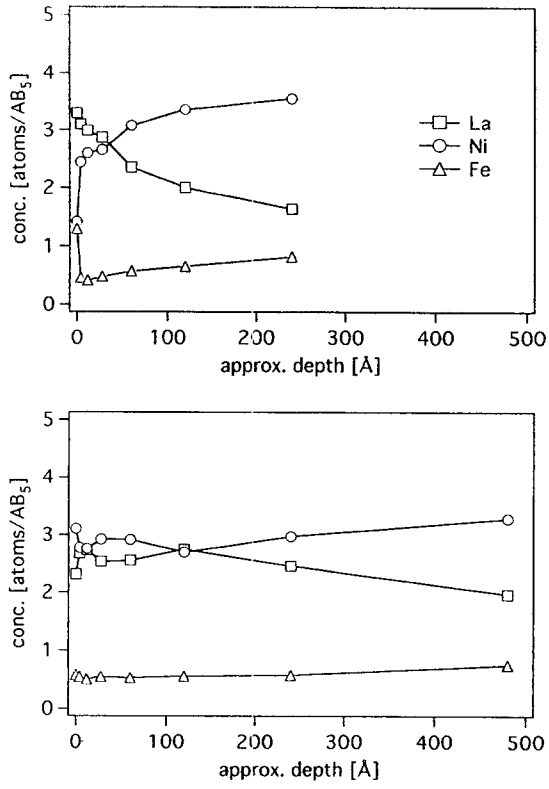

Fig. 8. XPS sputter depth profiles of $LaNi_4Fe$ showing the La, Ni and Fe concentrations. The top graph is for the original alloy and the bottom graph is for the alloy powder which has been electrochemically charge–discharge cycled 30 times.

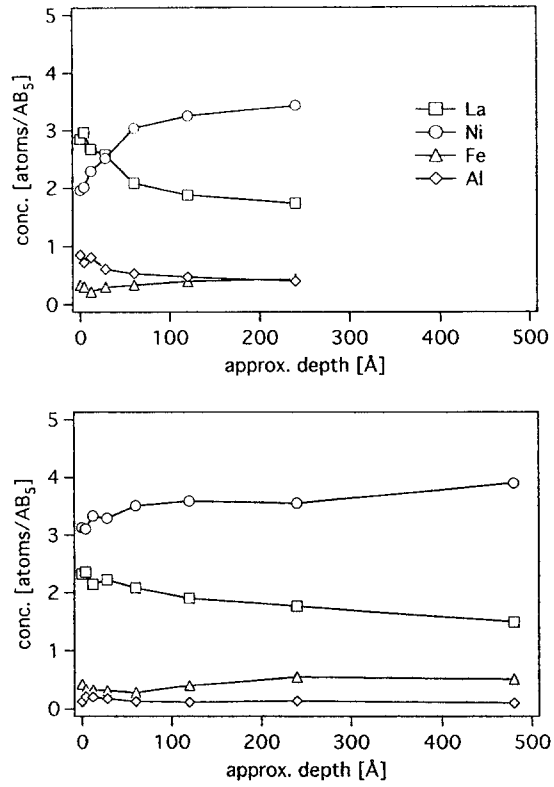

Fig. 9. XPS sputter depth profiles of $LaNi_{4.2}Fe_{0.5}Al_{0.3}$ showing the La, Ni, Fe and Al concentrations. The top graph is for the original alloy and the bottom graph is for the alloy powder which has been electrochemically charge–discharge cycled 30 times.

enrichment could be found for the cycled alloys. The nickel oxide thickness was in the same range as that found earlier for other cycled alloys, i.e. $LaNi_{4.7}Al_{0.3}$ (10 Å), $LaNi_5$ (20 Å) and $LaNi_{4.5}Si_{0.5}$ (4 Å) [13,14]. The nickel oxide and iron oxide thicknesses were largest for the $LaNi_4Fe$ sample after 30 electrochemical cycles. This sample already showed a considerable capacity loss after 30 cycles (Fig. 10).

4. Conclusions

We have found that iron substitution for nickel in $LaNi_5$ does not increase the electrochemical cycle life of the alloy, but a combined substitution of iron and aluminium does. The corrosion stability can be dramatically improved using mischmetal-based alloys. A capacity of 280 mAh g^{-1} was attained for $MmNi_{3.6}Fe_{0.7}Al_{0.3}Mn_{0.4}$. These alloys may be stable enough to release only minor amounts of iron into the electrolyte. In this case, they could be used as a cobalt-free metal hydride electrode together with an $Ni(OH)_2$ electrode without lowering the oxygen evolution potential.

The potential for the reduction of iron

$$Fe(OH)_2 + 2e^- \rightarrow Fe + 2OH^-$$

is at −0.975 V vs. Hg/HgO [15]. This value is more negative than the equilibrium electrode potential of the fully charged alloy electrode, which is about −0.950 V. With a charging current of 150 mA g^{-1}, the overpotential is 20 mV; for hydrogen evolution, it is 30 mV, which results in an electrode minimum potential of −0.980 V. It is unlikely that the oxidized iron is reduced at the end of the charge. Therefore reversible iron oxidation–reduction does not contribute to the electrode capacity.

Analysis by XPS of $LaNi_4Fe$ and $LaNi_{4.5}Fe_{0.5}$ samples demonstrated a change from a lanthanum oxide-rich to a nickel- rich surface layer after electrochemical cycling. The alloy with the better cyclic stability had a higher concentration of metallic nickel at the surface. Aluminium and iron showed approximately bulk concentrations at the surface of the cycled alloys. Iron does not seem to play a main role at the surface, except that it can reduce the usually observed strong nickel enrichment.

With iron-containing AB_5-type alloys it was possible

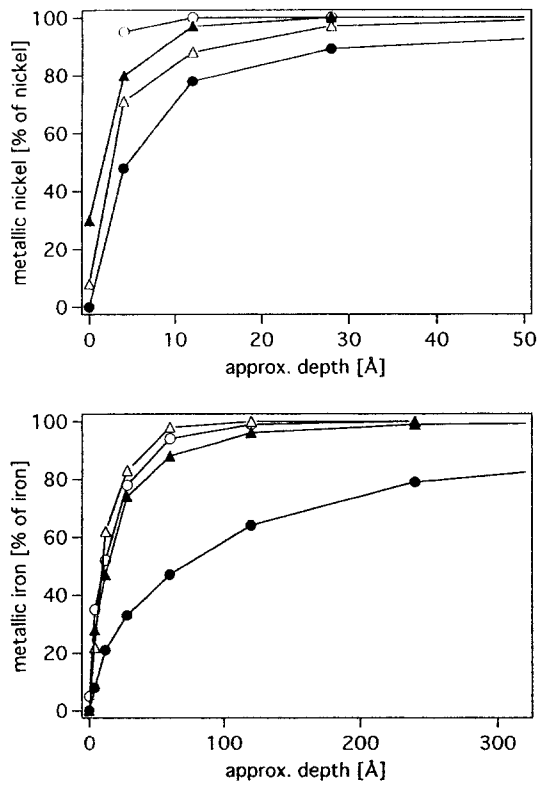

Fig. 10. Content of metallic nickel (top graph) and iron (bottom graph) as a percentage of the total element concentration (oxidized + metallic) as a function of the sputtered depth for $LaNi_4Fe$ (circles) and $LaNi_{4.2}Fe_{0.5}Al_{0.3}$ (triangles). The open symbols represent the original alloy and the filled symbols represent the alloy powders which have been electrochemically charge–discharge cycled 30 times.

to obtain good cyclic stability and a reasonably high capacity without using cobalt. These alloys have promising properties and should be tested in closed cells.

Acknowledgements

We gratefully acknowledge the help of Mr. Jörg Frischknecht with the XPS measurements and the financial support of the Swiss Department of Energy (BEW).

References

[1] T. Sakai, H. Miyamura, N. Kuriyama, H. Ishikawa and I. Uehara, *Z. Phys. Chem. (Neue Folge), 183* (1994) 333.

[2] (a) D.A. Corrigan and S. Srinivasan (eds.), *Proc. Symp. on Hydrogen Storage Materials, Batteries and Electrochemistry*, The Electrochemical Society, 1992. (b) H. Ogawa, M. Ikoma, H. Kawano and I. Matsumoto, *Power Sources, 12* (1989) 393.

[3] H.H. Van Mal, K.H.L. Buschow and A.R. Miedema, *J. Less-Common Met., 35* (1974) 65.

[4] G.D. Sandrock, *Proc. 2nd World Conf. on Hydrogen Energy Systems, Zürich, 1978*, Vol. 3, 1978, p. 1625.

[5] E.L. Huston and G.D. Sandrock, *J. Less-Common Met., 74* (1980) 435. (b) J. Lamloumi, A. Percheron Guegan, C. Lartigue, J.C. Achard and G. Jehonno, *J. Less-Common Met., 130* (1987) 111.

[6] K. Ohta, K. Hayashi, H. Matsuda, Y. Toyoguchi and M. Ikoma, *Extended Abstracts, Electrochemical Society Fall Meeting, Miami Beach, Florida, 1994*, The Electrochemical Society, 1994, p. 98.

[7] A. Züttel, F. Meli and L. Schlapbach, *Z. Phys. Chem. (Neue Folge), 183* (1994) 355.

[8] F. Meli, A. Züttel and L. Schlapbach, *J. Alloys Compounds, 202* (1993) 81.

[9] K. Hasegawa, M. Ohnishi, M. Oshitani, K. Takeshima, Y. Matsumaru and K. Tamura, *Z. Phys. Chem. (Neue Folge), 183* (1994) 325.

[10] F. Meli, A. Züttel and L. Schlapbach, *J. Alloys Compounds*, (1995).

[11] T. Sakai, M. Muta, H. Miyamura, N. Kuriyama and H. Ishikawa, *Electrochem. Soc. Proc., 93* (8) (1993) 240.

[12] T. Sakai, H. Miyamura, N. Kuriyama, I. Uehara, M. Muta, A. Takagi, U. Kajiyama, K. Kinoshita and F. Isogai, *J. Alloys Compounds, 192* (1993) 158.

[13] F. Meli and L. Schlapbach, *J. Less-Common Met., 172–174* (1991) 1252.

[14] F. Meli, A. Züttel and L. Schlapbach, *J. Alloys Compounds, 190* (1992) 17.

[15] C. Hamann and W. Vielstich, *Elektrochemie II*, Taschentext, Verlag Chemie, Weinheim, 1981.